RSC Advances

REVIEW

View Article Online
View Journal | View Issue

Cite this: *RSC Adv.*, 2024, **14**, 1417

Improving the stability of perovskite nanocrystals *via* SiO_2 coating and their applications

Qing-Feng Li, [a] Jin-Tao Wang *[a] and Zhenling Wang *[b]

Lead halide perovskite nanocrystals (LHP NCs) with outstanding optical properties have been regarded as promising alternatives to traditional phosphors for lighting and next-generation display technology. However, the practical applications of LHP NCs are seriously hindered by their poor stability upon exposure to moisture, oxygen, light, and heat. Hence, various strategies have been proposed to solve this issue. In this review, we have focused our attention on improving the stability of LHP NCs *via* SiO_2 coating because it has the advantages of simple operation, less toxicity, and easy repetition. SiO_2 coating is classified into four types: (a) *in situ* hydrolytic coating, (b) mesoporous silica loading, (c) mediated anchoring, and (d) double coating. The potential applications of SiO_2-coated LHP NCs in the field of optoelectronics, biology, and catalysis are presented to elucidate the reliability and availability of SiO_2 coating. Finally, the future development and challenges in the preparation of SiO_2-coated LHP NCs are analyzed in order to promote the commercialization process of LHP NC-related commodities.

Received 24th October 2023
Accepted 21st December 2023

DOI: 10.1039/d3ra07231b

rsc.li/rsc-advances

1. Introduction

Lead halide perovskite nanocrystals (LHP NCs) have attracted remarkable attention owing to their good optical performance, such as high luminescence quantum yields, tunable emission wavelength, high color purity, and long carrier diffusion length. These features make them promising for applications in next-generation photovoltaic and optoelectronic devices.[1–5] However, the major obstacles for such applications come from their poor chemical stability. Specifically, when LHP NCs are exposed to external environment, factors such as oxygen, polar solvent, light, and heat cause phase transformation and even structure degradation, resulting in serious photoluminescence (PL) quenching.[6–10] This problem is mainly attributed to two aspects: (1) the intrinsic ionic structure and low lattice energy of LHP NCs; (2) dynamic equilibrium between the adsorption and desorption of ligands on their surface.[11] Moreover, the halide anion exchange reaction between LHP NCs with different emitted colors upon mixing is another issue that hinders their practical application in multicolor display and lighting. Previous reports showed that when $CsPbBr_3$ and $CsPbI_3$ are mixed in a colloidal solution, they could be quickly cross-exchanged and homogenized within 2 min to form a $CsPb(Br/I)_3$ solid solution.[12] This phenomenon makes it difficult to prepare white light-emitting diodes (WLED) just by mixing perovskite nanocrystals with different halides in a single layer. Recently, Lu and coworkers proved that anion exchange was mainly driven by physical collision between perovskite nanocrystals.[13] SiO_2 coating can isolate perovskite nanocrystals from each other, thereby reducing the occurrence of anion exchange. Finally, lead is a toxic heavy metal, and exposure to it in the environment poses a variety of acute and chronic poisoning risks to humans. Lead can affect the genetic makeup, produce neurotoxicity, cause fetal toxicity during pregnancy or breast-feeding, and damage the kidneys as well as hematopoietic and immune systems. The toxicity of lead-containing perovskites also severely limits their commercialization.

Recently, extensive efforts have been devoted to solve the above issues. A routine method is to coat LHP NCs with an inert shell or incorporate them into barrier matrixes, which can (1) protect LHP NCs from moisture and oxygen, (2) passivate surface defects and enhance radiative recombination, as well as (3) prevent the halide anion exchange reaction and leakage of lead.[14–18] In particular, coating LHP NCs with an SiO_2 protective layer is considered to be the most practical way to improve their stability, where the SiO_2 protective layer is usually formed by the hydrolysis of organosilanes directly in water or exposed to ambient air.[19–28] Over the past five years, a number of reviews have summarized various methods to improve the stability of LHPs,[2,3] but systematic reviews on improving the stability of LHP NCs by SiO_2 coating are still lacking.

In this review, the origin of the instability of LHP NCs is discussed and the advantages of coating LHP NCs with SiO_2 as a protective layer is analyzed. Then, the recent advances of using SiO_2 coating to improve the stability of LHP NCs are summarized. SiO_2 coating is further subdivided into four types: *in situ* hydrolytic coating, mesoporous silica loading, mediated

[a]*Henan Key Laboratory of Rare Earth Functional Materials, International Joint Research Laboratory for Biomedical Nanomaterials of Henan, Zhoukou Normal University, Zhoukou, 466001, Henan, China. E-mail: wangjintao2565@126.com*

[b]*College of Materials Engineering, Henan International Joint Laboratory of Rare Earth Composite Materials, Henan University of Engineering, Xinzheng, 451191, China. E-mail: zlwang2007@hotmail.com*

anchoring, and double coating. The synthesis of monodisperse LHP NCs@SiO_2 core–shell (yolk–shell) composites is emphasized because it facilitates their application in the photoelectric and biological fields. Besides, some applications of SiO_2-coated LHP NCs in white light-emitting diodes, fluorescence imaging and detection, and catalysis are presented. Finally, the future development and challenges for the preparation of SiO_2-coated LHP NCs are briefly summarized and discussed.

2. SiO_2

SiO_2 is an inorganic compound composed of silicon atoms and oxygen atoms, in which the long-range ordered arrangement of silicon atoms and oxygen atoms can form crystalline SiO_2, while the short-range ordered or long-range disordered arrangement can form amorphous SiO_2. In particular, mesoporous SiO_2 has the characteristics of large specific surface area, strong surface adsorption and easy modifiability, good dispersion, as well as superior stability, widely used as the matrix or carrier to prepare composite materials.[29–32] Moreover, SiO_2 has proved to be one of the most promising candidates for encapsulating LHP NCs and improving their stability for the following reasons: (1) high chemical and thermal stability. SiO_2 has the characteristics of high temperature resistance, small thermal expansion coefficient, and corrosion resistance. (2) Non-toxicity. SiO_2 has the advantages of strong hydrophilicity and good biocompatibility, and is often used as a carrier for biosensors and biomarkers. (3) Easy modification. The SiO_2 surface is rich in the silicon hydroxyl group, which can be functionalized by the silanization reaction. (4) Tunable pore structure. With the aid of template agent and pore-forming agent, the pore size of silica can be adjusted to micropore, mesoporous, and macropore. This feature enables SiO_2 as a matrix to grow LHP NCs in its pores. (5) Low light absorption coefficient. SiO_2 is almost fully transparent in the visible light region.[33,34] (6) Strong imitability. SiO_2-coated luminescent materials, especially semiconductor quantum dots (QDs), have been extensively studied for nearly 20 years. The main synthetic methods include reversed-phase microemulsion method, "Stober" method, ship-in-a-bottle, and multi-shell coating. These mature techniques provide inspiration and reference for the research on SiO_2-coated perovskite QDs. Moreover, SiO_2-coating can not only reduce the toxicity and degradation of QDs but also prevent them from agglomerating, which affects their dispersibility and fluorescence properties. In addition, the interaction between SiO_2 and LHP NCs is considered to have special effects on the stability of LHP NCs. Thus, this review focuses on summarizing the preparation methods and applications of SiO_2-coated LHP NCs.

3. Preparation methods of SiO_2-coated LHP NCs

3.1 *In situ* hydrolytic coating

The main methods used to synthesize SiO_2-coated nanomaterials include reversed-phase microemulsion method and "Stober" method. However, both methods need to be performed in an alkaline aqueous environment, which will lead to the decomposition and fluorescence quenching of perovskite quantum dots (QDs). (3-Aminopropyl)triethoxysilane (APTES) is an amino-containing silane coupling agent. As a capping agent, APTES facilitates the dissolution of lead halide and the stabilization of the perovskite QDs.[35] The amino group of APTES can efficiently passivate the surface of perovskite QDs to maintain its high photoluminescence quantum yield (PLQY). Moreover, APTES can be naturally hydrolyzed to form a cross-linked SiO_2 matrix to cover the perovskite QDs by capturing trace amounts of water in organic solutions or air. Therefore, APTES can act as both the capping agent for perovskite QDs and the precursor for the formation an SiO_2 protective layer.[36–41] In 2016, Yu *et al.* synthesized a kind of perovskite QD/silica composites by adding APTES during perovskite NCs formation (Fig. 1a).[35] The obtained perovskite QD/silica composites exhibited high PLQY and extremely high stability in air (Fig. 1b). Most importantly, the anion-exchange phenomena between different perovskite QD/silica composites were not observed, which is conducive for fabricating the WLED devices. By integrating green- and red-emitting perovskite QD/silica composites with blue LED chips, a WLED with CIE color coordinates of (0.33, 0.33) and power efficiency of 61.2 lm W^{-1} was obtained (Fig. 1c and d), showing their potential in the field of white lighting.

Although traditional SiO_2 coating techniques can improve the stability and optical optoelectronic performance of perovskite NCs, they only achieve thick shells, which results in the aggregation of perovskite NCs in the bulk SiO_2 matrix, severely limiting the practical application. Since some optoelectronic and biomedical applications require the use of monodisperse nanoparticles rather than large aggregates, much efforts have been made toward exploring the techniques for coating perovskite NCs with SiO_2 at the single particle level. In 2018, Zhang and colleagues reported the preparation of monodisperse $CsPbBr_3$@SiO_2 core–shell nanoparticles in which only one $CsPbBr_3$ nanoparticles was encapsulated in the SiO_2 shell using a modified supersaturated recrystallization method (Fig. 1e).[42] In this research, the mixture of CsBr, $PbBr_2$, oleic acid, oleylamine, DMF, and ammonia solution was rapidly injected into an ultradry toluene containing tetramethoxysilane (TMOS), and then the formation process of $CsPbBr_3$@SiO_2 core–shell nanoparticles was carefully monitored by TEM. It was found that the capping reagent, reaction temperature, pH value, and precursor species were critical for the successful preparation of $CsPbBr_3$@SiO_2 core–shell nanoparticles. Due to the protection of the SiO_2 shell, $CsPbBr_3$@SiO_2 core–shell nanoparticles showed higher long-term stability in moist air and enhanced stability in water than that of bare $CsPbBr_3$ nanoparticles (Fig. 1f), which lays the foundation for its further application. However, the presence of ammonia solution could lead to the decomposition of $CsPbBr_3$ cores, and a small amount of fragmentation of $CsPbBr_3$ was observed in TEM images.

One of the challenges in SiO_2-coated perovskite NCs is that the surface capping ligands used to stabilize perovskite NCs enhance their hydrophobicity. Therefore, it is difficult to achieve hydrophilic SiO_2 coating on hydrophobic perovskite NCs. In 2021, Yang *et al.* proposed an ingenious method to solve this problem (Fig. 1g).[43] In step 1, tetramethoxysilane (TMOS) was

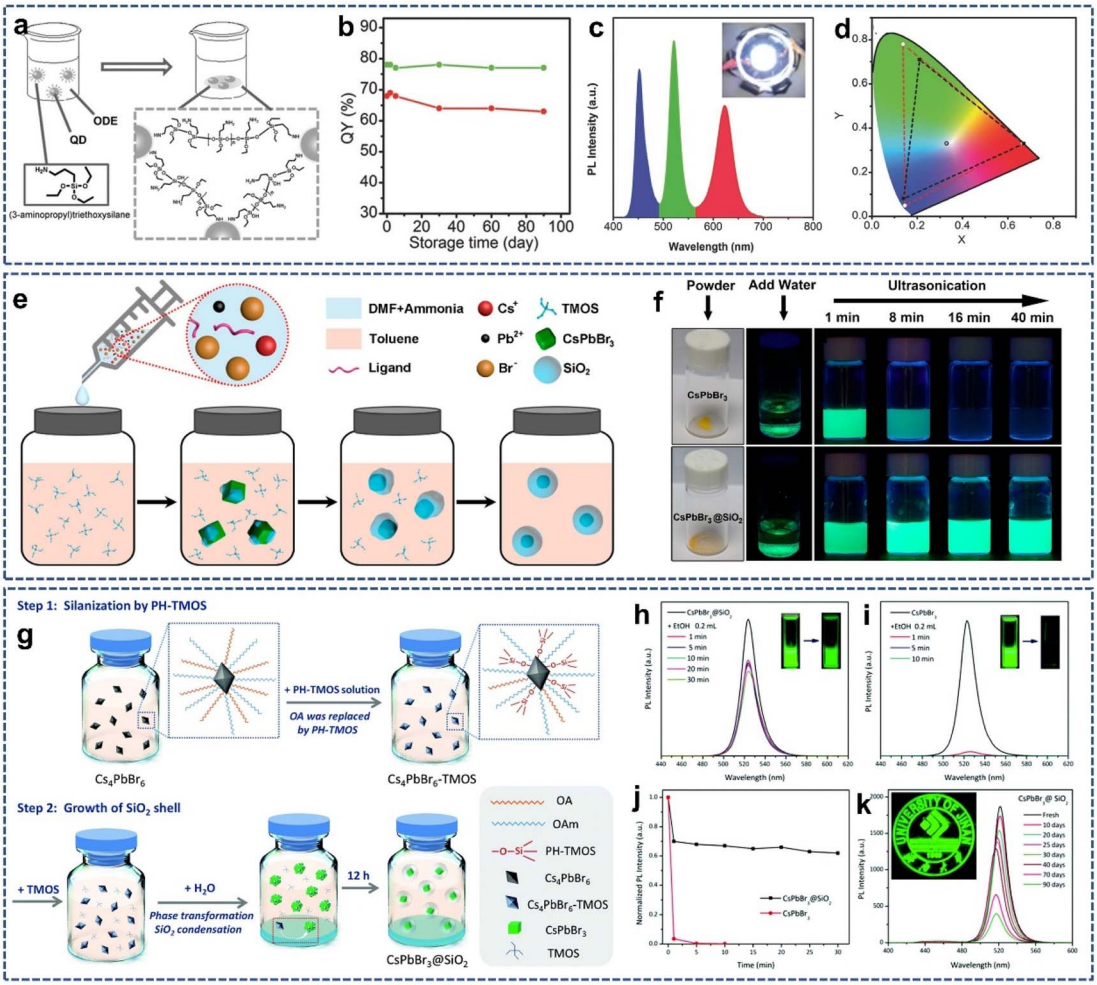

Fig. 1 (a) Schematic illustration of the preparation of QD/silica composites. (b) PLQY stability of the green and red QD/silica composites. (c) PL spectra of the WLED. (d) CIE color coordinates of the WLED device. Reproduced with permission from ref. 35. Copyright 2016 John Wiley and Sons. (e) Schematic illustration of the formation process of $CsPbBr_3$@SiO_2 core–shell NPs. (f) Photographs of the stability of the $CsPbBr_3$ NCs and $CsPbBr_3$@SiO_2 core–shell NPs against water. Reproduced with permission from ref. 42. Copyright 2018 American Chemical Society. (g) Schematic illustration of the preparation process of $CsPbBr_3$@SiO_2 capsules. PL spectra of the $CsPbBr_3$@SiO_2 (h) and $CsPbBr_3$ (i) solutions after adding EtOH. (j) Normalized PL intensity of the $CsPbBr_3$@SiO_2 and $CsPbBr_3$ after EtOH treatment. (k) PL intensity of the $CsPbBr_3$@SiO_2 film under ambient conditions over time. Reproduced with permission from ref. 43. Copyright 2021 The Royal Society of Chemistry.

partially hydrolyzed by controlling the added molar ratio of TMOS to water. Next, Cs_4PbBr_6 NCs was modified using the partially hydrolyzed TMOS (PH-TMOS) in which PH-TMOS was absorbed onto the surface of Cs_4PbBr_6 NCs *via* the Si–OH group to remove the hydrophobic oleic acid. In step 2, phase transformation from Cs_4PbBr_6 NCs into $CsPbBr_3$ NCs occurred after water injection. Meanwhile, the newly added TMOS underwent hydrolysis to generate the cross-linked Si–O–Si. Importantly, step 1 produced a large number of binding sites on the surface of perovskite NCs for the condensation of TMOS, which is conducive for the formation of $CsPbBr_3$@SiO_2. Benefiting from the protection of the SiO_2 layer, the prepared $CsPbBr_3$@SiO_2 showed better optical stability against polar solvents and air (Fig. 1h–k). But this SiO_2 coating technique did not block surface ion exchange on the perovskites, which brings obstacles to its application in the field of white light emitting diode (WLED).

3.2 Mesoporous silica loading

In the past two decades, mesoporous silica (m-SiO_2) with highly ordered structures, tunable narrow pore size distributions, and large specific surface area has aroused wide interest due to its great application potential in materials and life sciences. Due to the unique pore structure of m-SiO_2, guest molecules with different properties and sizes are easily loaded into the pore to form the host–guest functional materials through ion exchange, adsorption, and ship-in-bottle.[44–49] In 2016, Kovalenko and coworkers found that when the perovskite precursor solutions infiltrated into the pores of m-SiO_2, followed by drying, it would cause evaporation-induced crystallization in the formation of perovskite NCs within m-SiO_2 (Fig. 2a).[50] Because perovskite NCs have unique defect tolerance properties, they can be crystallized in the pore of m-SiO_2. Moreover, the prepared perovskite/m-SiO_2

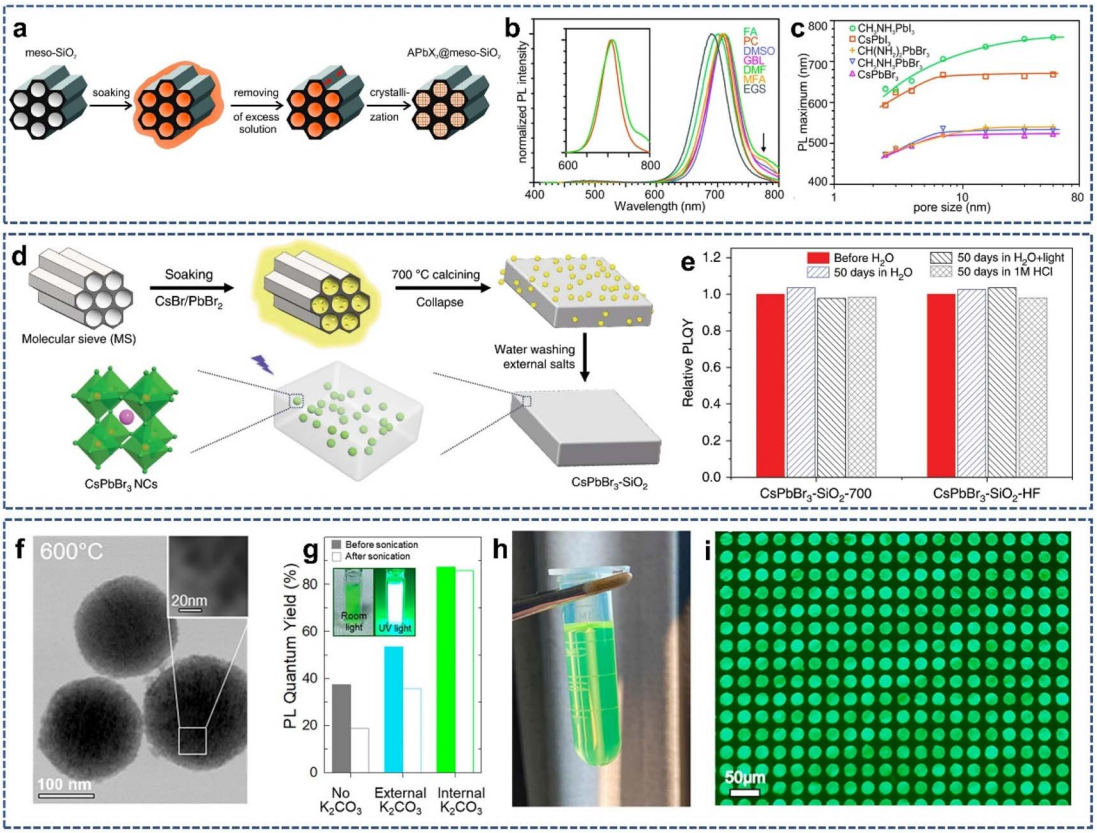

Fig. 2 (a) Schematic illustration of the template-assisted synthesis of $APbX_3$ NCs ($A = Cs^+$, $CH_3NH_3^+$ (MA) or $CH(NH_2)_2^+$ (FA); $X = Br^-$ or I^-) in the pores of mesoporous silica. (b) PL spectra of $MAPbI_3$ NCs synthesized from various solvents in 7 nm-SiO_2. (c) PL maximum as a function of template pore-size for various $APbX_3$ perovskite NCs grown in m-SiO_2. Reproduced with permission from ref. 50. Copyright 2016 American Chemical Society. (d) Schematic illustration of the synthesis $CsPbBr_3$ NCs into m-SiO_2. (e) Relative PLQYs of the $CsPbBr_3$–SiO_2-700 and $CsPbBr_3$–SiO_2–HF after immersion in various solvents for 50 days. Reproduced with permission from ref. 51. Copyright 2020 The Authors. (f) TEM image of the $CsPbBr_3$–SiO_2 NSs at 600 °C. (g) PLQY of the $CsPbBr_3$–SiO_2 NSs with different K_2CO_3 treatment before and after sonication in water. (h) Photograph of photolithographic ink fabricated by $CsPbBr_3$–SiO_2 NSs under room light. (i) Fluorescent image of 20 μm pixel array based on $CsPbBr_3$–SiO_2 NSs. Reproduced with permission from ref. 52. Copyright 2022 The Authors.

composites displayed excellent photoluminescence. By changing the pore size of m-SiO_2 (Fig. 2b) and solvent polarization (Fig. 2c), the emission band could be widely adjusted in the green to near-infrared band range, with the emission line widths down to 22 nm in the green and 36 nm in the red. This is an early report on the preparation of perovskite NCs/m-SiO_2 composite luminescent materials by the ship-in-bottle method. However, due to the open channel of m-SiO_2, the perovskite NCs in the channel of m-SiO_2 inevitably contacts with the external environment, leading to their limited long-range stability.

To solve this problem, Li *et al.* proposed a new strategy whereby m-SiO_2 was first soaked into the solutions of CsBr and $PbBr_2$, followed by drying at 80 °C. Next, the resulting solid was placed into a muffle furnace and heated to 600–900 °C at a heating rate of 5 °C min^{-1} in air atmosphere (Fig. 2d).[51] In this case, perovskite NCs were formed in the confined pores of m-SiO_2; meanwhile, the pore channel of m-SiO_2 gradually collapsed, finally forming an embedded, dense $CsPbBr_3/SiO_2$ composite. Fluorescence measurement showed that the as-prepared $CsPbBr_3$–SiO_2 has a high photoluminescence quantum yield (PLQY), up to 71% and a narrow emission of full width half peak at about 20 nm. In addition, because $CsPbBr_3$ NCs was completely sealed by dense SiO_2, $CsPbBr_3$–SiO_2 could maintain no significant photoluminescence intensity change for 50 days in hydrochloric acid solution (1 M HCl), proving that $CsPbBr_3$–SiO_2 powder possessed a very high stability against water and hydrochloric acid (Fig. 2e). However, the high temperature used in this synthesis can lead to the regrowth of SiO_2 particles, resulting in the formation of large particles or even bulk glasses, which limits their possible applications in practical devices because of poor dispersion in the solvent. Therefore, in order to achieve high stability and solution dispersion, it is necessary to develop a new pore sealing strategy that is more practical than high-temperature annealing, while preventing the particles from sintering together. Inspired by films or m-SiO_2 sintering methods that use low melting salts as the flux agent to initiate surface melting or particles binding through the solid/liquid interface, Li *et al.* synthesized solution-dispersible, uniform sized, highly luminescence, and ultra-stable $CsPbBr_3$–SiO_2 nanospheres ($CsPbBr_3$–SiO_2 NSs) by

selectively sintering m-SiO_2 nanoparticles loaded with the precursor of $CsPbBr_3$ (CsBr, $PbBr_2$) and low melting salts (K_2CO_3).[52] In particular, K_2CO_3 not only passivated the surface defects of $CsPbBr_3$ NCs but also promoted the complete collapse of internal pores of m-SiO_2 at an annealing temperature of 600 °C. The TEM images showed that SiO_2 nanospheres sintered at 600 °C maintained their original single-particle spherical morphology (Fig. 2f), indicating that this sintering temperature did not cause the aggregation of m-SiO_2 into bulk particles. Optical measurements displayed that the as-prepared $CsPbBr_3$–SiO_2 nanospheres had a high photoluminescence quantum yield (87 ± 5%, Fig. 2g) and narrow emission width (≈20 nm). Finally, the resulting $CsPbBr_3$–SiO_2 nanospheres were used as the basic material to make photolithographic ink for the fabrication of μ-LED conversion patterns with pixels less than 20 μm (Fig. 2h and i).

3.3 Mediated anchoring

It is widely known that the surface modification of SiO_2 with organosilanizing agent will enhance the interactions of SiO_2 with other materials. Moreover, amino and carboxyl groups possess strong binding with perovskite quantum dot (QDs). Therefore, amino and carboxyl-modified SiO_2 can provide specific sites for the nucleation and growth of perovskite QDs, thus significantly reducing fluorescence degradation and improving the stability of perovskite QDs.[53,54] In 2017, Zeng *et al.* reported a one-pot and universal strategy for the synthesis of highly luminescent, environmentally stable $CsPbBr_3$ QDs/A-SiO_2 composite powders by amino-mediated anchoring of perovskite QDs to SiO_2 surfaces (Fig. 3a).[55] Also, the emission wavelength could be tuned over the entire visible region by changing the anion composition (Fig. 3b). In addition, the photostability of perovskite QDs was greatly improved by separating perovskite QDs from each other and inhibiting the light-induced QDs regrowth. Thus, 80% photoluminescence intensity was maintained after 108 h of continuous UV light exposure (Fig. 3c), and little photoluminescence degradation was observed after 40 days of storage under ambient conditions (Fig. 3d). An extremely stable random laser was also achieved after 2 months of storage or continuous optical pumping for 8 h.

However, from the above method, perovskite QDs are only anchored on the surface of amino-modified SiO_2, and the external water molecules can still intrude on perovskite QDs. Recent studies have shown that the mediated anchoring of perovskite QDs on the hydrophobic SiO_2 surface will improve the moisture resistance of perovskite QDs. In 2019, Liu *et al.* developed a highly stable perovskite $CsPbBr_3$ NCs composite ($CsPbBr_3$@CA-SiO_2) obtained by the *in situ* growth of $CsPbBr_3$ NCs grown on octadecyl/propylamine-coated SiO_2 nanowires (Fig. 3e and f).[56] In this case, octadecyl/propylamine-coated SiO_2 nanowires were first prepared in water/oil emulsion using an anisotropic sol–gel growth method. The octadecyl group on the SiO_2 surface provided a hydrophobic environment, while the amino group served as the surface ligand, coordinating the precursors (Pb^{2+} or Cs^+) to form nucleation sites and templating the formation of $CsPbBr_3$@CA-SiO_2. Next, the suspension of $CsPbBr_3$@CA-SiO_2 and toluene was cast onto a compact filter paper and filtered under reduced pressure to obtain the $CsPbBr_3$@CA-SiO_2-based membrane. As expected, the $CsPbBr_3$@CA-SiO_2-based membrane exhibited excellent de-wetting and high hydrophobicity with a water contact angle of 162° and showed excellent stability toward water, heat, and UV irradiation (Fig. 3g–j).

3.4 Double coating

As mentioned above, SiO_2 coating has been shown to be an effective strategy for improving the stability of perovskite QDs. In addition, strategies such as hydrophobic polymer embedding can also improve the stability of perovskite QDs. Hence, it is reasonable to envisage the combination of SiO_2 coating with other embedding methods to enhance the stability of perovskite QDs.[57–59] In 2019, Chen *et al.* reported a dual protection strategy to embed perovskite QDs in double hydrophobic shells of alkyl-functionalized SiO_2 and hydrophobic poly(vinylidene fluoride) (PVDF) to improve the stability of perovskite QDs (Fig. 4a).[60] During the synthesis, the perovskite precursor solution was first infiltrated in the cavity of hollow alkyl-functionalized SiO_2 *via* capillary forces. Next, PVDF wrapped around the alkyl-functionalized SiO_2 through hydrophobic interactions. Finally, the perovskite QDs capped with hydrophobic SiO_2 and PVDF shells were obtained after vacuum drying. Under the dual protection of hydrophobic SiO_2 and PVDF shell, the as-synthesized perovskite QDs composite ($MAPbBr_3$@SiO_2/PVDF) showed long-term storage and significantly improved the stability against moisture, air, and UV irradiation (Fig. 4b–d). Also, a white light-emitting diode (WLED) was fabricated by combining green emitting $MAPbBr_3$@SiO_2/PVDF with red-emitting K_2SiF_6:Mn^{4+} on blue-emitting GaN chips (Fig. 4e), exhibiting a luminescence efficiency of 147.5 lm W^{-1} and a color gamut of 120% of the National Television System Committee standard. However, the photoluminescence intensity of $MAPbBr_3$@SiO_2/PVDF decreased obviously after being immersed in water, indicating that the hydrophobic SiO_2 and PVDF shells are not completely dense and that the external water molecules can still penetrate the dual protective shells under harsh conditions.

Recently, many reports have shown that high-temperature sintering can achieve a dense protective layer with few pinholes and good barrier properties.[46,61] However, it is a challenge to improve the stability of perovskite QDs using two dense inorganic protective layers obtained by high-temperature sintering. In 2022, Bi *et al.* proposed a one-pot method for the synthesis of high stable inorganic double-protected perovskite QDs composites ($CsPbBr_3$@$PbSO_4$/SiO_2), in which $CsPbBr_3$ QDs were embedded in the sintered SiO_2 matrix and further coated with $PbSO_4$ shell (Fig. 4f).[62] In this process, the SiO_2 matrix not only provides a sufficient space for the growth of perovskite QDs but can also be densified under high temperature sintering. At the same time, $PbSO_4$ can be formed *in situ* on the surface of $CsPbBr_3$

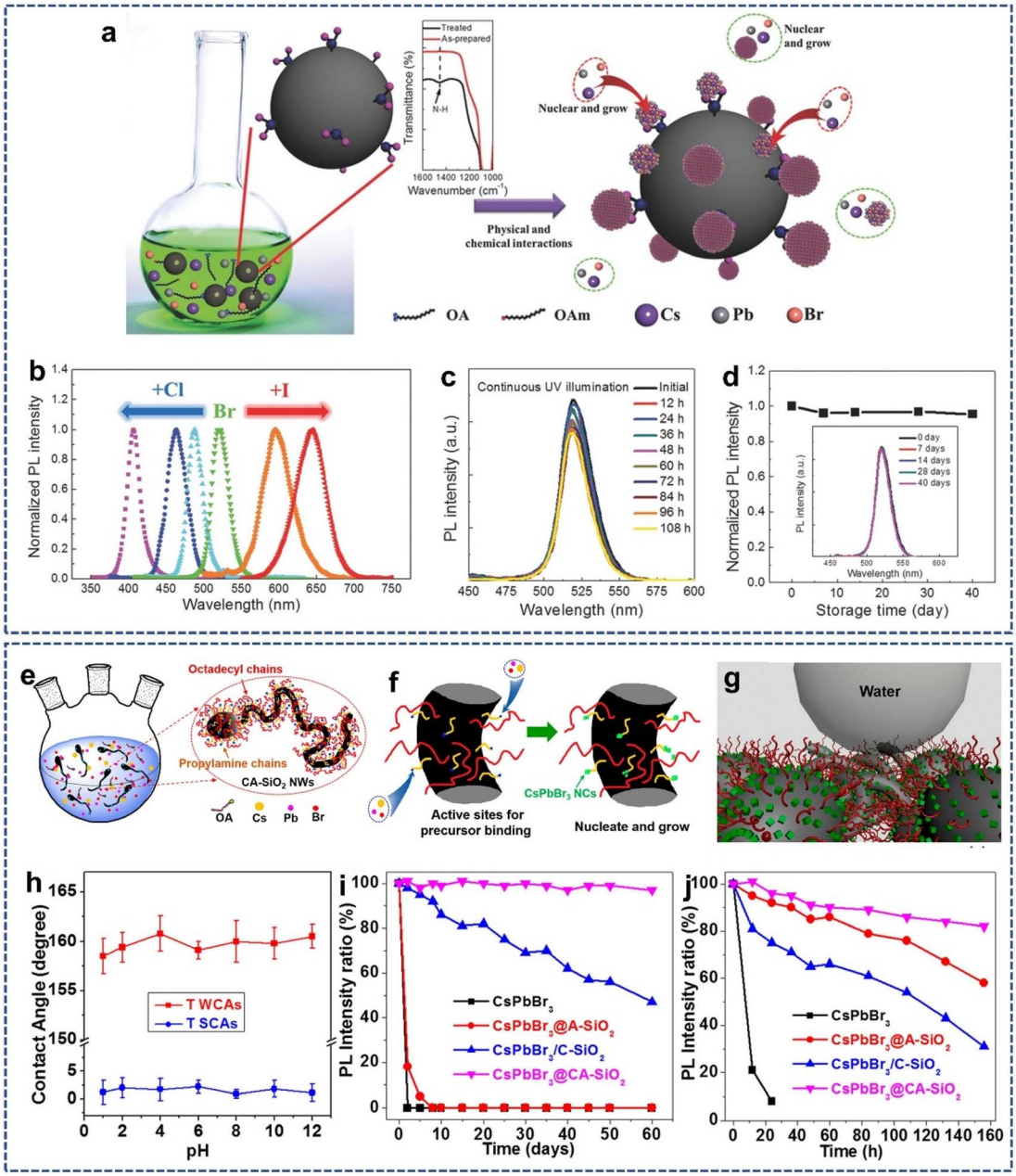

Fig. 3 (a) Schematic illustration of the fabrication of perovskite/A-SiO_2. (b) Adjustable photoluminescence *via* anion modulation. (c) PL spectra of the $CsPbBr_3$ QDs/A-SiO_2 composites as functions of UV light illumination. (d) Stability of the $CsPbBr_3$ QDs/A-SiO_2 composites after storage without any protection. Reproduced with permission from ref. 55. Copyright 2017 John Wiley and Sons. (e and f) Schematic illustration of the construction strategy and growing process of $CsPbBr_3$@CA-SiO_2 composites. (g) Schematic illustration of the $CsPbBr_3$@CA-SiO_2 membrane for enhanced stability and de-wetting property. (h) Plot of water contact angles of the $CsPbBr_3$@CA-SiO_2 membrane at different pH values. Relative PLQY plots (i) against the time being immersed in water and (j) against different UV irradiation times for composites. Reproduced with permission from ref. 56. Copyright 2018 American Chemical Society.

QDs by high-temperature induced reaction, which further passivates and protects $CsPbBr_3$ QDs. However, the formation of the $PbSO_4$ shell was unexpected because no SO_4^{2-} was added in the experiment. A reasonable explanation is that DMSO, as the only sulfur source, underwent a gas phase reaction at high temperature and transformed into SO_4^{2-}, inducing the formation of $PbSO_4$ on the surface of $CsPbBr_3$. Thanks to the dual protective effects of SiO_2 and $PbSO_4$ shells, $CsPbBr_3$@$PbSO_4$/SiO_2 could maintain its excellent PL intensity after 1 year of immersion in water (Fig. 4g). In addition, $CsPbBr_3$@$PbSO_4$/SiO_2 could survive in concentrated aqueous HCl solution and HBr aqueous solution for 25 days (Fig. 4h) and 500 °C for 24 h (Fig. 4i), indicating that the dual inorganic protective shells prevent the decomposition and anion exchange of $CsPbBr_3$.

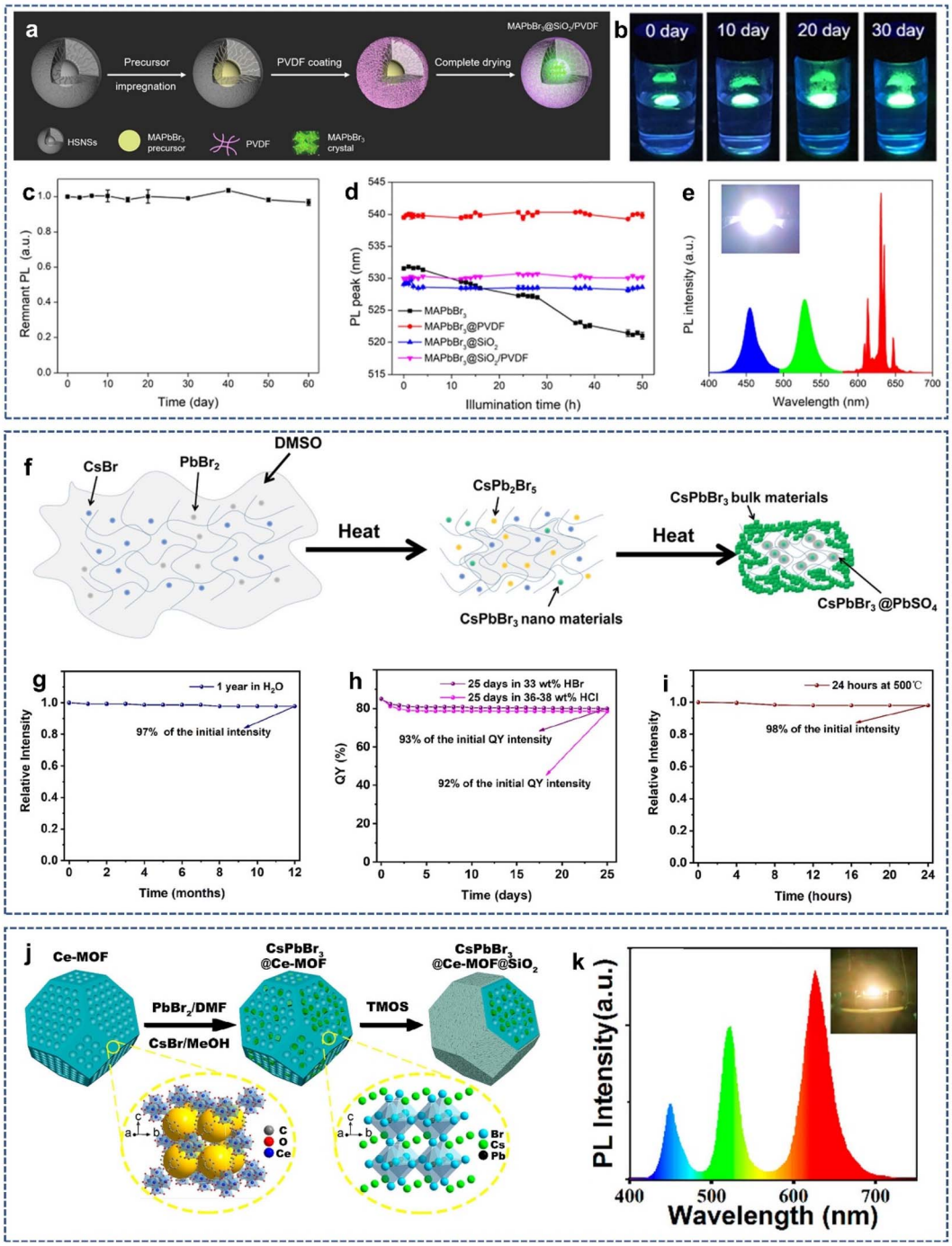

Fig. 4 (a) Schematic illustration of the preparation process of $MAPbBr_3@SiO_2$/PVDF NPs. (b) Photographs of the stability of $MAPbBr_3@SiO_2$/PVDF NPs floating on water for 30 days. (c) PL intensity of $MAPbBr_3@SiO_2$/PVDF NPs under ambient conditions for 60 days. (d) Changes in the PL peaks of the $MAPbBr_3$-based films with illumination time. (e) Emission spectra of the WLED. Reproduced with permission from ref. 60. Copyright 2019 American Chemical Society. (f) Schematic illustration of the formation mechanism of $CsPbBr_3@PbSO_4/SiO_2$. Water stability (g), stability in HCl and HBr solution (h), and thermal stability (i) of the sample. Reproduced with permission from ref. 62. Copyright 2022 American Chemical Society. (j) Schematic illustration of the fabrication process of $CsPbBr_3$@Ce-MOF@SiO_2 composites. (k) Emission spectrum and corresponding photograph of the white $CsPbX_3$@Ce-MOF@SiO_2 LED. Reproduced with permission from ref. 63. Copyright 2022 American Chemical Society.

As newly developed crystalline porous materials, metal–organic frameworks (MOFs) have ultra-high porosity and large internal surface area, which endows them with great application potential in gas storage and separation, luminescence, sensing, catalysis, magnetism, and other fields. In particular, the diverse porous structure, high structural stability, and good compatibility also make MOFs good matrixes for loading guest species such as drugs,

nanoclusters, and semiconductor QDs. In recent years, MOFs have been widely used in the encapsulation of perovskite QDs to improve the stability. However, the pore structure of MOFs used for loading perovskite QDs is still open to the environment, which will expose perovskite QDs to external environmental factors, such as water and oxygen. In 2022, Wang *et al.* proposed a dual encapsulation strategy to prepare monodisperse $CsPbX_3$@Ce-MOF@SiO_2 composites by the growth of $CsPbX_3$ QDs *in situ* in mesoporous Ce-MOF, followed by silane hydrolysis-encapsulation (Fig. 4j).[63] The as-prepared $CsPbX_3$@Ce-MOF@SiO_2 showed high luminescence yield, which benefits from the waveguiding effect of the Ce-MOF mesoporous structure, thus inhibiting the self-reabsorption losses of perovskite QDs. Moreover, the dual protective shells effectively blocked the perovskite QDs from the external environment so that $CsPbX_3$@Ce-MOF@SiO_2 composites exhibited greatly enhanced stability against heat, UV light, air, and halide ion. $CsPbX_3$@Ce-MOF@SiO_2 composites allowed for the flexible regulation of the band gap by controlling the ratio of Cl/Br/I in the precursor. Therefore, the emission color of $CsPbX_3$@Ce-MOF@SiO_2 composites could be tuned throughout the entire visible region. By combining green-emitting and red-emitting $CsPbX_3$@Ce-MOF@SiO_2 composites with blue-emitting InGaN chip, a warm white light LED could be obtained (Fig. 4k), showing their potential application in the optoelectronics field.

To facilitate the comparison between different synthesis strategies, the synthesis, stability, size, and LED characteristics of several SiO_2-coated perovskite NCs are summarized in Table 1.

4. Applications of SiO_2-coated LHP NCs

4.1 White light-emitting diodes

Perovskite QDs is a new type of photoelectric materials, which has the advantages of high fluorescence quantum efficiency, high brightness, high defect tolerance, and color gamut meeting the BT.2020 standard. Environmental instability is the main obstacle to their application, but this problem can be solved by oxide coating.[64,65] In 2020, Costa *et al.* developed a dual oxide-coated $CsPbBr_3$@SiO_2/ZrO_2 composite by kinetically controlling the sol–gel reaction of APTES and zirconium *tert*-butoxide. The perovskite-converted hybrid light-emitting diodes (pc-HLEDs) fabricated by $CsPbBr_3$@SiO_2/ZrO_2 displayed a high efficiency of 75 lm W^{-1} and stabilities of ≈200 and 700 h operating at 100 and 10 mA, respectively.[66] However, long exposure to moisture under continuous blue excitation still hinders the long-term stability of the device, probably because the protective shell prepared by the sol–gel method is not completely dense. In 2021, Manna *et al.* proposed a molten salt-assisted sintering strategy to synthesize the high stability of the $CsPbBr_3$/m-SiO_2 composite (Fig. 5a).[67] In this case, the pores of

Table 1 The synthesis, stability, size, and LED characteristics of the SiO_2-coated perovskite NCs

Sample	Synthesis	Stability	Size/structure	LED characteristics	Ref.
QD/silica composites	One step *in situ* coating	PL QY decays by less than 5% after 90 days storage	Bulk	PL intensity is hardly reduced after 10 h of continuous illumination	35
$CsPbBr_3$@SiO_2 core–shell NPs	One step *in situ* coating	PL intensity increases by 12% after 40 min of ultrasound	18.2 nm/core–shell		42
$CsPbBr_3$@SiO_2 NCs	Two-step coating	PL intensity declines to 62% after immersion in ethanol for 30 min	47 nm/core–shell		43
Meso-SiO_2-templated $CsPbBr_3$	Limit-domain growth in mesopore	PLQY remains unchanged after 6 days of UV lamp irradiation	0.5–1 μm particles with ordered 1D-channels of 7 nm in diameter		50
$CsPbBr_3$–SiO_2–HF	Limit-domain growth in mesopore/sintering	PLQY remains unchanged after immersion in water for 50 days	Bulk	PL intensity maintains 100% after 1000 h of continuous illumination	51
$CsPbX_3$–SiO_2 NSs	Limit-domain growth in mesopore/K_2CO_3 assisted sintering	PL intensity remains unchanged after sonication in water for 20 h	200 ± 26 nm	PL intensity maintains 94% after 1000 h of continuous illumination	52
$CsPbBr_3$ QDs/A-SiO_2	Amino-mediated anchoring	PL intensity remains unchanged after 40 days storage in air	≈250 nm		55
$CsPbBr_3$@CA-SiO_2	Amino-mediated anchoring	PL intensity decays by less than 5% after immersion in water for 60 days	5–10 μm/nanowire		56
$MAPbBr_3$@SiO_2/PVDF	Double coating with SiO_2 and PVDF	PL intensity decays by 3% after 40 days storage in air	20.7 nm/core–shell	The WLED exhibits a luminous efficiency of 147.5 lm W^{-1}	60
$CsPbBr_3$@$PbSO_4$/SiO_2	Double coating with SiO_2 and $PbSO_4$	PL intensity decays by 3% after immersion in water for one year	Bulk		62
$CsPbBr_3$@Ce-MOF@SiO_2	Double coating with SiO_2 and Ce-MOFs	PL intensity decays by 24% after 60 days storage	500 nm/octahedron	The WLED exhibits a luminous efficiency of 87.8 lm W^{-1}	63

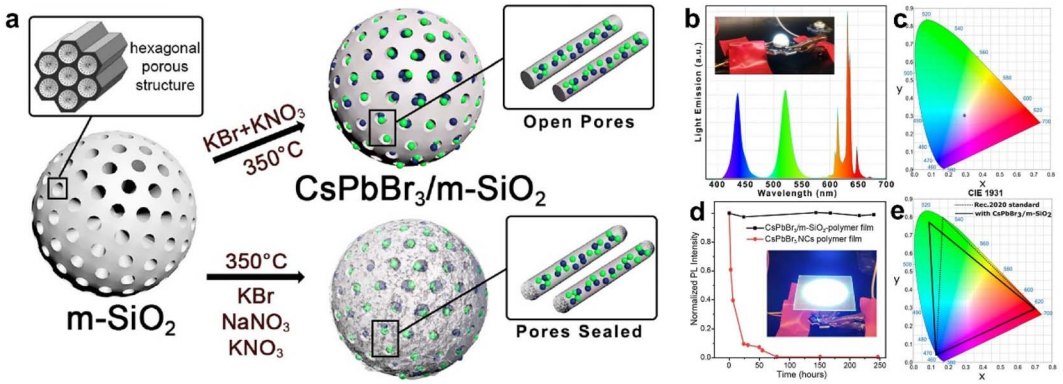

Fig. 5 (a) Schematic illustration of the preparation of $CsPbBr_3$/m-SiO_2 composites. Emission spectrum (b) and corresponding CIE1931 color coordinate diagram (c) of the fabricated W-LED. (d) Time-dependent normalized PL intensity of the $CsPbBr_3$/m-SiO_2 polymer film and standard $CsPbBr_3$ NCs polymer film under high flux remote application test. (e) Color coverage of the $CsPbBr_3$ NCs-polymer composite film as compared to the standard Rec.2020 area. Reproduced with permission from ref. 67. Copyright 2021 The Authors.

the SiO_2 protective layer were sealed, thus conferring a high stability to the $CsPbBr_3$/m-SiO_2 composite. Moreover, utilizing $CsPbBr_3$/m-SiO_2 as a green color emitter for a white LED was capable of generating a white light with a correlated color temperature (CCT) of 7692 K (Fig. 5b–e). These results indicate that perovskite QDs have broad application prospects in the field of light-emitting diode.

4.2 Fluorescence imaging and detection

Over the past years, the rapid development of fluorescence imaging and detection technology has provided a great opportunity for early warning and differential diagnosis of diseases. Also, fluorescence probes are the key to realize fluorescence imaging and detection. Recent studies have found that perovskite QDs with high luminescence quantum yields, narrow emission band, and broad spectral tunability are good candidates for the fluorescence probes.[68–74] But the following issues need to be addressed: (1) water stability. A common way to improve the poor water stability of perovskite QDs is to use inert SiO_2 as a protective shell to encapsulate or coat perovskite QDs. (2) Water dispersibility. The hydrophilic surface and small size favor particle dispersion; thus, the monodisperse perovskite@SiO_2 composites are good for bioimaging and detection. (3) Biotoxicity. Silica coating can mitigate lead leakage and reduce the biological and environmental toxicity of perovskite QD. In 2020, Park *et al.* developed a highly luminescent biocompatible $CsPbBr_3$@SiO_2 core–shell nanoprobe for bioimaging and drug delivery.[75] The thickness of the SiO_2 shell around the $CsPbBr_3$ core could be tuned from 9 to 51 nm by controlling the coating time, resulting in an increase in the size of the $CsPbBr_3$@SiO_2 core–shell nanoprobe from 70 to 210 nm. The $CsPbBr_3$@SiO_2 core–shell nanoprobe showed high water stability and good biocompatibility, making it suitable for fluorescence-mediated bioimaging and detection. Confocal fluorescence images showed that the $CsPbBr_3$@SiO_2 core–shell nanoprobe induced endocytosis to HeLa cells (Fig. 6a), allowing the treated HeLa cells to exhibit green fluorescence upon 488 nm light excitation (Fig. 6b). Moreover, doxorubicin (Dox) could be physically adsorbed on the shell of the $CsPbBr_3$@SiO_2 core–shell nanoprobe and efficiently delivered to the nuclei of HeLa cells (Fig. 6c and d). But the SiO_2 shell of the $CsPbBr_3$@-SiO_2 core–shell nanoprobe is not dense and contains a large number of mesoporous; thus, the long-term stability and toxicity of the $CsPbBr_3$@SiO_2 core–shell nanoprobe need to be studied.

In 2021, Xu *et al.* reported the synthesis of polymer surface ligand and SiO_2 coating perovskite QDs ($CsPbBr_3$-mPEG@SiO_2) for efficient glutathione (GSH) detection (Fig. 6e).[76] The methoxypolyethylene glycolamine (mPEG-NH_2) ligand and SiO_2 encapsulation effectively passivated the perovskite QDs, greatly enhancing its fluorescence emission intensity and water stability. Moreover, the fluorescence of $CsPbBr_3$-mPEG@SiO_2 could be effectively quenched by Hg^{2+} ions, which is explained by the dynamic quenching model. But the fluorescence was restored after the addition of GSH in $CsPbBr_3$-mPEG@SiO_2 + Hg^{2+} solution, which is mainly derived from the strong interaction of glutathione with GSH. Thus, the "on–off–on" type fluorescence detection system based on $CsPbBr_3$-mPEG@SiO_2 can be established to achieve an efficient detection of GSH (Fig. 6f).

4.3 Catalysis

Today, the energy crisis has become a global problem. Since Fujishima and Honda first reported TiO_2 photocatalytic water splitting to produce hydrogen,[77] photocatalysis has evolved into an efficient and green technique that can solve these problems. In the last decade, an emerging semiconductor material, lead halide perovskite, shows great potential in photocatalysis applications due to its low band gap energy and high photon-to-electron conversion capability.[78–80] In 2022, Li *et al.* reported the synthesis of $CsPbBr_3$/$CsPb_2Br_5$@silica yolk–shell composite microspheres for the photocatalytic degradation of dyes (Fig. 7a).[81] The authors found that precisely controlling the composition of perovskite precursors (Cs^+ and Pb^{2+} ratio) could form the $CsPbBr_3$/$CsPb_2Br_5$ heterostructure with different ratios in mesoporous SiO_2 hollow spheres. XRD was performed to evaluate the stability of $CsPbBr_3$/$CsPb_2Br_5$@silica after

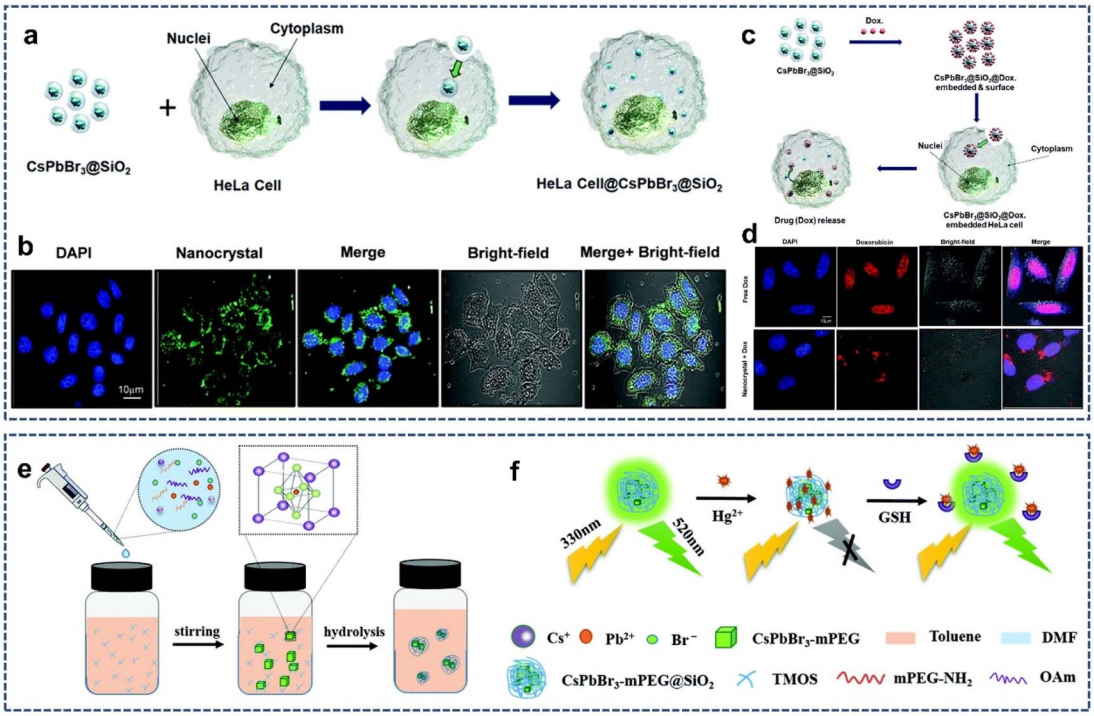

Fig. 6 (a) Schematic illustration of the proposed mechanism of endocytosis induced by the $CsPbBr_3$@SiO_2 core–shell nanoprobe. (b) Confocal fluorescence image of HeLa cells after incubation with the $CsPbBr_3$@SiO_2 core–shell nanoprobe. (c) Schematic illustration of the proposed mechanism of drug loading and release in the $CsPbBr_3$@SiO_2@Dox-embedded HeLa cells. (d) Confocal fluorescence image of HeLa cells after incubation with Dox-loaded $CsPbBr_3$@SiO_2 core–shell nanoprobe. Reproduced with permission from ref. 75. Copyright 2020 The Royal Society of Chemistry. (e) Schematic illustration of the synthesis of the $CsPbBr_3$-mPEG@SiO_2. (f) "On–off–on" type fluorescence sensing of Hg^{2+} and GSH. Reproduced with permission from ref. 76. Copyright 2021 The Royal Society of Chemistry.

photocatalysis. After one cycle of photocatalysis, no obvious miscellaneous peaks appeared in the XRD pattern, indicating that most of the $CsPbBr_3/CsPb_2Br_5$ is still in the SiO_2 shell. Moreover, TEM revealed the formation of the heterojunction between $CsPbBr_3$ and $CsPb_2Br_5$, which likely improves the carrier dissociation and transport for the photocatalytic reaction. The photodegradation of Rhodamine B showed that $CsPbBr_3/CsPb_2Br_5$@silica has higher photocatalytic activities than commercial P25.

Over the past two decades, the photocatalytic reduction of CO_2 to C1 compounds has aroused great interest because C1 obtained by reducing CO_2 can be further converted into clean fuels such as ethanol and acetic acid. In 2023, Wang *et al.* synthesized a $Cs_2AgBiBr_6$@SiO_2 yolk–shell composite *via* a ship-in-a-bottle technology for water-stable photocatalytic CO_2 reduction (Fig. 7b).[82] The SiO_2 protective layer gave $Cs_2AgBiBr_6$ good thermal stability and photostability as well as good corrosion resistance to polar solvents. To evaluate the performance of photocatalytic CO_2 reduction, model experiments were performed in a mixture of acetonitrile and water under visible light irradiation with $Cs_2AgBiBr_6$@SiO_2 as the catalyst, $Co(bpy)_3^{2+}$ (bpy = 2,2′-bipyridine) as the co-catalyst, and triethanolamine as the hole scavenger. It was found that CO_2 was mainly reduced to CO, with a little H_2 generated as the byproduct. Also, the CO-evolution rate was measured as 271.76 μmol g^{-1} h^{-1}, indicating that $Cs_2AgBiBr_6$@SiO_2 has a high CO_2 photoreduction performance (Fig. 7c).

Photocatalytic organic synthesis is a promising green synthesis method that can use light energy to excite the catalyst, thereby achieving specific organic reactions under mild conditions. In recent years, numerous studies have shown that lead halide perovskites can effectively activate the C–H bond under light irradiation for subsequent transformations.[83,84] In 2020, Tüysüz *et al.* reported a strategy for the selective activation of aliphatic and aromatic C–H bonds using supported bismuth halide perovskite photocatalysts.[85] The photocatalyst ($Cs_3Bi_2Br_9$/SBA-15) was prepared using the incipient wetness impregnation method. The well-dispersed halide perovskite nanoparticles (2–5 nm) were confined to the mesoporous SBA-15 matrix, which allowed for better electron–hole separation and tighter contact with hydrocarbons. Under visible light irradiation, $Cs_3Bi_2Br_9$/SBA-15 could effectively oxidize the saturated C–H bonds of various hydrocarbons to the corresponding oxygenates (mainly aldehydes/ketones), with a conversion rate up to ~32 900 μmol g_{cat}^{-1} h^{-1} and high selectivity >99% (Fig. 7d). Mechanistic studies showed that photo-induced hole (h^+) cleaved the saturated C–H bonds to form carbon-centered radicals, which further reacted with O_2 to form oxygenated compounds (Fig. 7e). In contrast to most studies on C–H bond activation that closely focus on benzyl or allyl positions, this study achieves the activation of aliphatic C–H, which greatly expands the use of perovskite as the photocatalyst in organic synthesis.

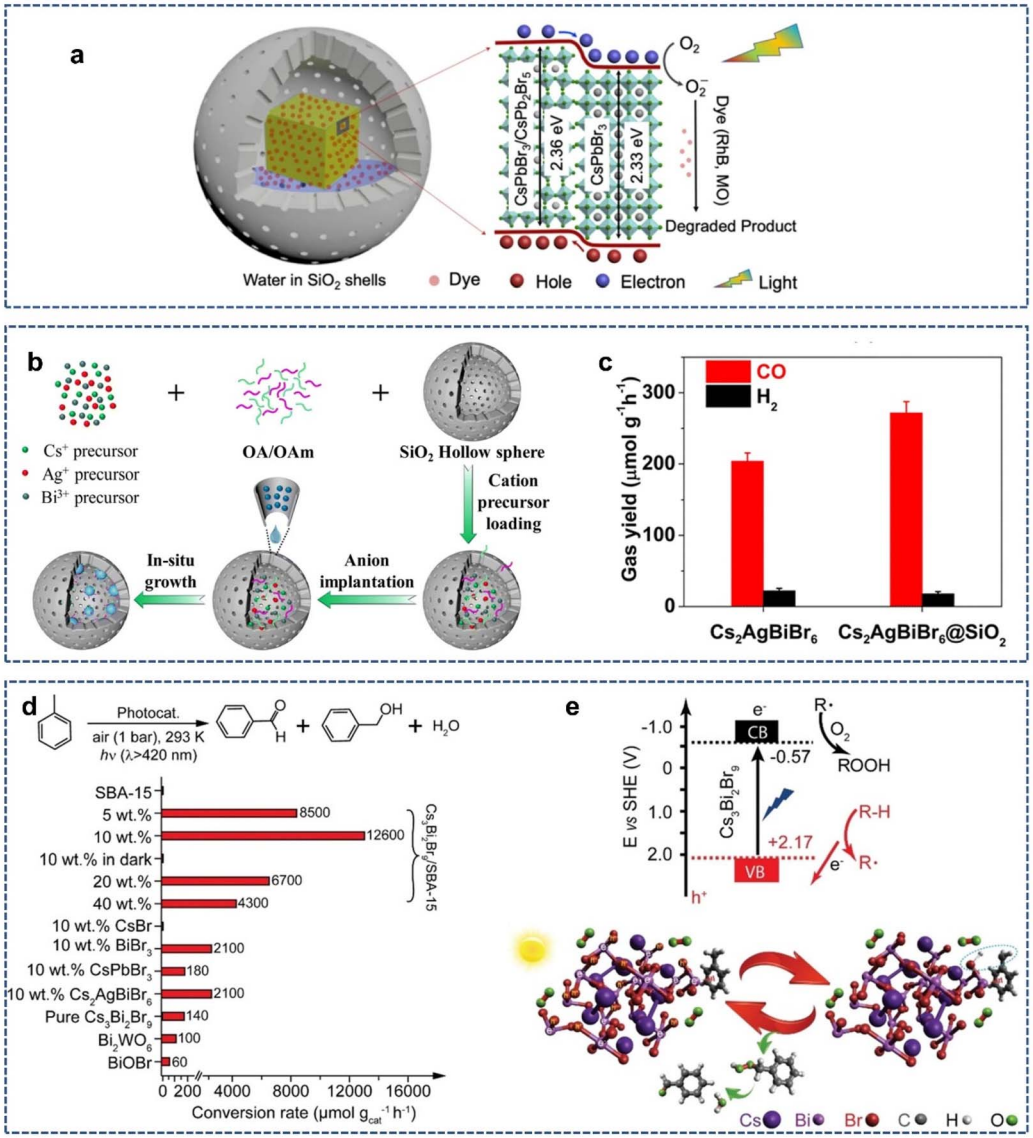

Fig. 7 (a) The photocatalytic mechanism diagram of dye degradation by the $CsPbBr_3/CsPb_2Br_5$@silica yolk–shell composite microspheres. Reproduced with permission from ref. 81. Copyright 2022 The Authors. (b) Schematic illustration of the synthesis of the $Cs_2AgBiBr_6@SiO_2$ yolk–shell composites. (c) Formation rates of photocatalytic reduction of CO_2 to CO and H_2 over $Cs_2AgBiBr_6$ nanocrystals and $Cs_2AgBiBr_6@SiO_2$. Reproduced with permission from ref. 82. Copyright 2023 The Royal Society of Chemistry. (d) Photocatalytic oxidation of toluene over diverse catalysts. (e) Energy diagram and proposed mechanism of supported $Cs_3Bi_2Br_9$ nanoparticles for $C(sp^3)$–H bond activation. Reproduced with permission from ref. 85. Copyright 2019 The Authors.

5. Conclusions and outlooks

As a new semiconductor material, LHP NCs display fascinating optical and electronic performance, making them ideal candidates for light-emitting and display devices. But their commercial applications are seriously hindered by the poor stability, toxicity, and anion exchange. In particular, owing to their high intrinsic ion mobility and dynamic ligand binding, LHP NCs can undergo phase transition or structural decomposition upon exposure to moisture, oxygen, and UV light. Given the huge application potential of LHP NCs to be exploited, the stability of LHP NCs has become a prominent problem to be solved. SiO_2 coating is an effective method to improve the stability of LHP NCs with the advantages including less technical risk, low cost, and good repeatability. The review summarizes four methods to improve the stability of LHP NCs by SiO_2 coating: (1) *in situ* hydrolytic coating, (2) mesoporous silica loading, (3) mediated anchoring, (4) double coating. The *in situ* growth of LHP NCs in mesoporous SiO_2 by a ship-in-a-bottle technology is considered as a convenient method for preparing monodisperse LHP NCs@SiO_2 core–shell (yolk–shell) composites, which are conducive for practical application in optoelectronic and biological fields.

Despite many significant progresses that have been made in the synthesis of SiO_2-coated LHP NCs, some important problems still need to be addressed in the future. (1) The cost of

preparing silica-coated perovskite NCs with organosilane as a raw material is high. Relatively cheap commercial silicon-based raw materials, such as diatomite and kaolin, can be explored to coat perovskite NCs. (2) The large-scale preparation of SiO_2-coated LHP NCs for photoelectric application is still missing, which has greatly hindered the commercialization process. One step *in situ* preparation method may enable the large-scale preparation of the SiO_2-coated perovskite NCs. (3) High temperature can eliminate the pinhole of the SiO_2 shell but makes it easy to regrow SiO_2 to form large particles; thus, simultaneously controlling the SiO_2 shell density and the monodispersity of SiO_2-coated LHP NCs is a challenge. Low-temperature salt-assisted sintering method provides the possibility to solve this issue. (4) Double coating LHP NCs with SiO_2 and other oxides or non-oxides can not only improve the stability of LHP NCs but also give the composites novel properties. Among them, TiO_2, Al_2O_3, and ZnS are worth exploring. With the unremitting efforts of the researchers, we believed that the SiO_2 coating technology will provide opportunities for the development and commercialization of LHP NCs.

Conflicts of interest

There are no conflicts to declare.

Acknowledgements

This work was financially supported by the Youth Backbone Teacher Training Project of Henan Province (2020GGJS213) and Key Research Project of Henan Higher Education Institute (21A150066).

References

1 J. Shamsi, A. S. Urban, M. Imran, L. De Trizio and L. Mann, *Chem. Rev.*, 2019, **119**, 3296–3348.
2 Y. Wei, Z. Cheng and J. Lin, *Chem. Soc. Rev.*, 2019, **48**, 310–350.
3 W. Lv, L. Li, M. Xu, J. Hong, X. Tang, L. Xu, Y. Wu, R. Zhu, R. Chen and W. Huang, *Adv. Mater.*, 2019, **31**, 1900682.
4 M. V. Kovalenko, L. Protesescu and M. I. Bodnarchuk, *Science*, 2017, **358**, 745–750.
5 Z. Andaji-Garmaroudi, M. Anaya, A. J. Pearson and S. D. Stranks, *Adv. Energy Mater.*, 2020, **10**, 1903109.
6 Y. Xu, X. Hu, H. Tang, Q. Hu, S. Wang, T. Chen, X. Zhang, W. Jiang, L. Wang and W. Jiang, *Nanoscale*, 2023, **15**, 631–643.
7 H. Shankar, S. Ghosh and P. Kar, *J. Mater. Chem. C*, 2022, **10**, 11532–11554.
8 C. G. Sanjayan, M. S. Jyothi and R. G. Balakrishna, *J. Mater. Chem. C*, 2022, **10**, 6935–6956.
9 N. S. Peighambardoust, E. Sadeghi and U. Aydemir, *ACS Appl. Nano Mater.*, 2022, **5**, 14092–14132.
10 A. Mishra, R. Bose, Y. Zheng, W. Xu, R. McMullen, A. B. Mehta, M. J. Kim, J. W. P. Hsu, A. V. Malko and J. D. Slinker, *Adv. Mater.*, 2022, **34**, 2203226.
11 Y. Wang, J. Ren, X. Zhou and G. Zhang, *Mater. Chem. Front.*, 2023, **7**, 2175–2207.
12 G. Nedelcu, L. Protesescu, S. Yakunin, M. I. Bodnarchuk, M. J. Grotevent and M. V. Kovalenko, *Nano Lett.*, 2015, **15**, 5635–5640.
13 Y. C. Su, Q. Jing, Y. Xu, X. Xing and Z. D. Lu, *ACS Omega*, 2019, **4**, 22209–22213.
14 E. V. Kolobkova, R. Semaan, M. S. Kuznetsova and N. V. Nikonorov, *J. Lumin.*, 2023, **255**, 119541.
15 P. Wang, Z. H. Wu, M. Y. Wu, J. Wei, Y. N. Sun and Z. F. Zhao, *J. Mater. Sci.*, 2021, **56**, 4161–4171.
16 A. R. Yusoff, M. Vasilopoulou, D. G. Georgiadou, L. C. Palilis, A. Abate and M. K. Nazeeruddin, *Energy Environ. Sci.*, 2021, **14**, 2906–2953.
17 R. X. Li, B. B. Li, X. Fang, D. K. Wang, Y. Q. Shi, X. Liu, R. Chen and Z. P. Wei, *Adv. Mater.*, 2021, **33**, 2100466.
18 G. Y. Ding, Y. F. Zheng, X. Xiao, H. Y. Cheng, G. D. Zhang, Y. F. Shi and Y. C. Shao, *J. Mater. Chem. A*, 2022, **10**, 8159–8171.
19 S. Son, S. Jeon, D. Chae, S. Y. Lee, Y. Liu, H. Lim, S. J. Oh and H. Lee, *Nano Energy*, 2021, **79**, 105461.
20 Q. X. Zhong, M. H. Cao and Q. Zhang, *Nanoscale*, 2021, **13**, 19341–19351.
21 C. Rossi, R. Scarfiello, R. Brescia, L. Goldoni, G. Caputo, L. Carbone, D. Colombara, L. De Trizio, L. Manna and D. Baranov, *Chem. Mater.*, 2022, **34**, 405–413.
22 D. Chen, G. Fang and X. Chen, *ACS Appl. Mater. Interfaces*, 2017, **9**, 40477–40487.
23 F. Zhang, Z. F. Shi, S. Li, Z. Z. Ma, Y. Li, L. T. Wang, D. Wu, Y. T. Tian, G. T. Du, X. J. Li and C. X. Shan, *ACS Appl. Mater. Interfaces*, 2019, **11**, 28013–28022.
24 S. Park, M. N. An, G. Almeida, F. Palazon, D. Spirito, R. Krahne, Z. Dang, L. De Trizioa and L. Manna, *Nanoscale*, 2019, **11**, 18739–18745.
25 H. Lee, C. K. Trinh, M. G. So and C. L. Lee, *Nanoscale*, 2022, **14**, 3425–3440.
26 G. H. Ahmed, J. Yin, O. M. Bakr and O. F. Mohammed, *ACS Energy Lett.*, 2021, **6**, 1340–1357.
27 B. Shi, J. Lü, Y. Liu, Y. Xiao and C. Lü, *Mater. Chem. Front.*, 2021, **5**, 4343–4354.
28 Z. Liu, Y. Zhang, Y. Fan, Z. Chen, Z. Tang, J. Zhao, Y. Lv, J. Lin, X. Guo, J. Zhang and X. Liu, *ACS Appl. Mater. Interfaces*, 2018, **10**, 13053–13061.
29 R. K. Kankala, Y. H. Han, J. Na, C. H. Lee, Z. Sun, S. B. Wang, T. Kimura, Y. S. Ok, Y. Yamauchi, A. Z. Chen and K. C. W. Wu, *Adv. Mater.*, 2020, **32**, 1907035.
30 F. C. Lin, Y. Xie, T. Deng and J. I. Z. Magnetism, *J. Am. Chem. Soc.*, 2021, **143**, 6025–6036.
31 P. Díez, E. Lucena-Sánchez, A. Escudero, A. Llopis-Lorente, R. Villalonga and R. Martínez-Máñez, *ACS Nano*, 2021, **15**, 4467–4480.
32 A. Guerrero-Martínez, J. Pérez-Juste and L. M. Liz-Marzán, *Adv. Mater.*, 2010, **22**, 1182–1195.
33 A. M. Alsaad, A. A. Ahmad, A. R. Al Dairy, A. S. Al-anbar and Q. M. Al-Bataineh, *Results Phys.*, 2020, **19**, 103463.
34 G. L. Tan, M. F. Lemon and R. H. French, *J. Am. Ceram. Soc.*, 2003, **86**, 1885–1892.

35 C. Sun, Y. Zhang, C. Ruan, C. Yin, X. Wang, Y. Wang and W. W. Yu, *Adv. Mater.*, 2016, **28**, 10088–10094.
36 J. Cheng, S. Yuan, L. Zhu, L. Chen, C. Liu, H. Tong and H. Zeng, *Langmuir*, 2020, **36**, 6017–6024.
37 A. Pan, Y. Li, Y. Wu, K. Yan, M. Jurow, Y. Liu and L. He, *Mater. Chem. Front.*, 2019, **3**, 414–419.
38 C. K. Trinh, H. Lee, M. G. So and C. L. Lee, *ACS Appl. Mater. Interfaces*, 2021, **13**, 29798–29808.
39 S. Y. Lee, S. Jeon, J. Ahn, J. Bang, H. K. Woo, K. Lee, B. K. Jung, T. Park, D. Son, J. P. Ahn and S. J. Oh, *Appl. Surf. Sci.*, 2021, **563**, 150229.
40 A. V. Fulari, A. Jana, J. Han, S. Yeon, Y. Park, S. Cho, V. G. Sree, S. Park, H. Kim and H. Im, *J. Colloid Interface Sci.*, 2023, **630**, 212–222.
41 M. R. Kar, S. Ray, B. K. Patra and S. Bhaumik, *Mater. Today Chem.*, 2021, **20**, 100424.
42 Q. Zhong, M. Cao, H. Hu, D. Yang, M. Chen, P. Li, L. Wu and Q. Zhang, *ACS Nano*, 2018, **12**, 8579–8587.
43 M. Li, X. Zhang and P. Yang, *Nanoscale*, 2021, **13**, 3860–3867.
44 V. Malgras, S. Tominaka, J. W. Ryan, J. Henzie, T. Takei, K. Ohara and Y. Yamauchi, *J. Am. Chem. Soc.*, 2016, **138**, 13874–13881.
45 Y. Lin, X. Zheng, Z. Shangguan, G. Chen, W. Huang, W. Guo, X. Fan, X. Yang, Z. Zhao, T. Wu and Z. Chen, *J. Mater. Chem. C*, 2021, **9**, 12303–12313.
46 Y. Xu, L. Yu, K. Peng, Y. Deng, Y. Zhao, X. Zeng and Y. Yu, *Luminescence*, 2023, **38**, 536–545.
47 Y. Huang, Z. Lai, J. Jin, F. Lin, F. Li, L. Lin, D. Tian, Y. Wang, R. Xie and X. Chen, *Small*, 2021, **17**, 2103425.
48 V. Malgras, J. Henzie, T. Takei and Y. Yamauchi, *Angew. Chem., Int. Ed.*, 2018, **57**, 8881–8885.
49 M. Anaya, A. Rubino, T. C. Rojas, J. F. Galisteo-López, M. E. Calvo and H. Míguez, *Adv. Opt. Mater.*, 2017, **5**, 1601087.
50 D. N. Dirin, L. Protesescu, D. Trummer, I. V. Kochetygov, S. Yakunin, F. Krumeich, N. P. Stadie and M. V. Kovalenko, *Nano Lett.*, 2016, **16**, 5866–5874.
51 Q. Zhang, B. Wang, W. Zheng, L. Kong, Q. Wan, C. Zhang, Z. Li, X. Cao, M. Liu and L. Li, *Nat. Commun.*, 2020, **11**, 31.
52 M. He, Q. Zhang, F. Carulli, A. Erroi, W. Wei, L. Kong, C. Yuan, Q. Wan, M. Liu, X. Liao, W. Zhan, L. Han, X. Guo, S. Brovelli and L. Li, *ACS Energy Lett.*, 2023, **8**, 151–158.
53 Y. Guo, J. Chen, Y. Zhao and Y. Lou, *ChemSusChem*, 2022, **15**, e202200793.
54 J. Ren, X. Zhou and Y. Wang, *Chem. Eng. J.*, 2023, **454**, 140285.
55 X. Li, Y. Wang, H. Sun and H. Zeng, *Adv. Mater.*, 2017, **29**, 1701185.
56 A. Pan, M. J. Jurow, Y. Wu, M. Jia, F. Zheng, Y. Zhang, L. He and Y. Liu, *ACS Appl. Nano Mater.*, 2019, **2**, 258–266.
57 L. Xu, J. Chen, J. Song, J. Li, J. Xue, Y. Dong, B. Cai, Q. Shan, B. Han and H. Zeng, *ACS Appl. Mater. Interfaces*, 2017, **9**, 26556–26564.
58 S. Wang, D. Chen, K. Xu, J. Hu, D. Huang, M. Hong and H. Zhu, *Nano Res.*, 2023, **16**, 10507–10514.
59 L. Qiu, H. Yang, Z. Dai, F. Sun, J. Hao, M. Guan, P. Dang, C. Yan, J. Lin and G. Li, *Inorg. Chem. Front.*, 2020, **7**, 2060–2071.
60 Y. Huang, F. Li, L. Qiu, F. Lin, Z. Lai, S. Wang, L. Lin, Y. Zhu, Y. Wang, Y. Jiang and X. Chen, *ACS Appl. Mater. Interfaces*, 2019, **11**, 26384–26391.
61 H. Zhao, K. Kordas and S. Ojala, *J. Mater. Chem. A*, 2023, **11**, 22656–22687.
62 J. Han, D. Xu, C. Sun, H. Zhang, T. Wei, J. Tao, C. Fan and W. Bi, *ACS Appl. Energy Mater.*, 2022, **5**, 13461–13469.
63 J. Ren, A. Meijerink, X. Zhou, J. Wu, G. Zhang and Y. Wang, *ACS Appl. Mater. Interfaces*, 2022, **14**, 3176–3188.
64 Y. He, L. Zhang, G. Chen, Y. Liu, S. Shi, P. Jiang, J. Ding, S. Xu and C. Geng, *Appl. Surf. Sci.*, 2023, **611**, 155724.
65 X. Tang, W. Chen, Z. Liu, J. Du, Z. Yao, Y. Huang, C. Chen, Z. Yang, T. Shi, W. Hu, Z. Zang, Y. Chen and Y. Leng, *Small*, 2019, **15**, 1900484.
66 Y. Duan, C. Ezquerro, E. Serrano, E. Lalinde, J. García-Martínez, J. R. Berenguer and R. D. Costa, *Adv. Funct. Mater.*, 2020, **30**, 2005401.
67 M. N. An, S. Park, R. Brescia, M. Lutfullin, L. Sinatra, O. M. Bakr, L. De Trizio and L. Manna, *ACS Energy Lett.*, 2021, **6**, 900–907.
68 W. Xue, J. Zhong, H. Wu, J. Zhangc and Y. Chi, *Analyst*, 2021, **146**, 7545–7553.
69 S. Lou, Z. Zhou, T. Xuan, H. Li, J. Jiao, H. Zhang, R. Gautier and J. Wang, *ACS Appl. Mater. Interfaces*, 2019, **11**, 24241–24246.
70 S. Huang, Z. C. Yu, J. L. Xie, A. Wang, J. K. Li, Y. Meng and J. L. Song, *ChemistrySelect*, 2023, **8**, e202300176.
71 C. Collantes, V. G. Pedro, M. J. Bañuls and Á. Maquieira, *ACS Appl. Nano Mater.*, 2021, **4**, 2011–2018.
72 L. Cheng, J. Chi, M. Su and Y. Song, *J. Mater. Chem. C*, 2023, **11**, 7970–7981.
73 H. Lian, Y. Li, S. Saravanakumar, H. Jiang, Z. Li, J. Wang, L. Xu, W. Zhao and G. Han, *Coord. Chem. Rev.*, 2022, **452**, 214313.
74 H. Wu, Y. Chen, W. Zhang, M. S. Khan and Y. Chi, *ACS Appl. Nano Mater.*, 2021, **4**, 11791–11800.
75 P. Kumar, M. Patel, C. Park, H. Han, B. Jeong, H. Kang, R. Patel, W. G. Koh and C. Park, *J. Mater. Chem. B*, 2020, **8**, 10337–10345.
76 Y. Shu, L. Sun, Y. Wang, D. Jin, Q. Xu and X. Hu, *Analyst*, 2021, **146**, 6798–6807.
77 A. Fujishima and K. Honda, *Nature*, 1972, **238**, 37–38.
78 Y. Y. Duan, D. Y. Wang and R. D. Costa, *Adv. Funct. Mater.*, 2021, **31**, 2104634.
79 H. Mai, D. Chen, Y. Tachibana, H. Suzuki, R. Abe and R. A. Caruso, *Chem. Soc. Rev.*, 2021, **50**, 13692–13729.
80 S. Chen, H. Yin, P. Liu, Y. Wang and H. Zhao, *Adv. Mater.*, 2023, **35**, 2203836.
81 K. Xie, S. Wei, A. Alhadhrami, J. Liu, P. Zhang, A. Y. Elnaggar, F. Zhang, M. H. H. Mahmoud, V. Murugadoss, S. M. El-Bahy, F. Wang, C. Li and G. Li, *Adv. Compos. Hybrid Mater.*, 2022, **5**, 1423–1432.
82 J. Liu, Z. Wu, F. Zhang, M. Zhao, C. Li, J. Li, B. Wen and F. Wang, *Nanoscale*, 2023, **15**, 7023–7031.

83 W. B. Wu, Y. C. Wong, Z. K. Tan and J. Wu, *Catal. Sci. Technol.*, 2018, **8**, 4257–4263.
84 H. W. Huang, H. F. Yuan, J. W. Zhao, G. Solís-Fernández, C. Zhou, J. W. Seo, J. Hendrix, E. Debroye, J. A. Steele, J. Hofkens, J. L. Long and M. B. J. Roeffaers, *ACS Energy Lett.*, 2019, **4**, 203–208.
85 Y. T. Dai, C. Poidevin, C. Ochoa-Hernández, A. A. Auer and H. Tüysüz, *Angew. Chem., Int. Ed.*, 2020, **59**, 5788–5796.